Supporting Information

Grishchuk *et al*. 10.1073/pnas.0801811105

SI Text

Part 1: Additional Materials and Methods

Reagents and Experimental Conditions. Dam1 complex was prepared at 0.5–1 μM; the stoichiometry of Alexa488 labeling in different preps was 1.9–2.1 moles of dye per mole of protein. The concentration of soluble Dam1 was determined from its optical density at 280 nm (assumed extinction coefficient 10^5 M/cm). Each thawed aliquot of Alexa488-Dam1 was used for 2–4 days (kept on ice and protected from light). Late in this time window, more protein was required to obtain the same degree of MT decoration, suggesting that some activity was lost over time, so we used the fluorescence of MT-bound Dam1 as a guide to assess the amount of Dam1 protein to add. We analyzed data obtained with protein from different days after thawing and found no statistically significant differences in their behavior, so the results from different days were pooled. In experiments with proteins from different preparations (e.g., wild type vs. mutant) the amount of added protein was chosen such that it decorated MTs with a similar density of dots. For example, S4D-Dam1 was used at 30 nM to produce visible MT decoration, consistently with the reduced formation of oligomeric complexes by this mutant protein.

Work with Dam1-Coated Beads. Streptavidin (Pierce) was conjugated to carboxylated silica beads using the protocol provided by Bangs Laboratories. The streptavidin-coated beads (silica or plastic) were then incubated with biotinylated anti-penta-His antibodies (Qiagen) for 45 min at room temperature or for 1 h at 4°C. After washing and a brief treatment in the bath of a sonic cleaner (Branson, model 3510), $1.4{\cdot}10^8$ beads were incubated for 1–3 h at 4°C with 5–300 nM 6His-Dam1 complex, labeled with Alexa488. The latter protein bound to these beads when anti-penta-His antibodies were used, but not when biotinylated IgG (Jackson Immunoresearch) was used as a control. The beads were then washed twice in BRB80 supplemented with 1 mM DTT and 60–120 μM BSA at a bead concentration of 0.01% by mass and kept on ice for 1–4 days. Immediately before their use, the beads were washed twice more, as above.

To estimate the maximum density of Dam1 conjugation, after Dam1 had been allowed to bind to the beads via the above protocol, the beads were spun in a microcentrifuge, and the supernatant with unbound Dam1 was collected and combined with a fresh sample of beads coated with anti-penta-His antibodies. The fluorescent intensity of these beads was ~20% of the intensity of the beads incubated with Dam1 first, suggesting that the initial binding adsorbed ~80% of the soluble Dam1. The maximal Dam1 density we could achieve was $2–4{\cdot}10^4$ hetero-decamers/bead; lower levels of Dam1 conjugation were obtained by using more diluted Dam1 solutions. Reduced conjugation was confirmed by measuring bead fluorescence intensity. The minimum density that allowed the beads to move with depolymerizing MTs was 20–40 complexes per bead; such beads bound to MTs inefficiently, but some tethered and/or moving beads could be found.

To coat the beads unevenly with Alexa488-Dam1 we created a monolayer of the 0.97 μm beads, which had been evenly coated with anti-penta-His antibodies, by brief centrifugation in the filter devices (Pall corp.). Alexa488-Dam1 was added carefully to the beads, so that the monolayer was not disturbed, and incubated for 10 min. After the fluorescent Dam1 was washed away, beads were resuspended and then incubated with a saturating concentration of unlabeled Dam1, as described above.

Imaging and Data Acquisition. All light microscopic observations were made at 32°C on a Zeiss Axiophot2. Images were acquired with a Photometrics Cascade 650 CCD camera (Roper Scientific) equipped with a remote fan. Images of moving Dam1 complexes were acquired as z-stacks (3–4 planes 0.3 μm apart) to ensure that different parts of the MT appeared in focus, because the free, plus MT end was always deeper in the chamber than the coverglass-attached portion of the MT. The planes in best focus were then selected manually and used for further analysis with Metamorph 6.1 (Universal Imaging). This program was also used to track positions of both the beads and the Dam1 fluorescence. To enable a comparison of signal brightness during spot movement, integrated spot intensity was measured in constant areas that encompassed a distal MT tip, in control regions, such as non-moving dots, and in the image background. After subtracting the background, the intensity of the moving dot was divided by that of the control dot, to compensate for bleaching. Supporting information (SI) Movie S1 and Movie S2 were assembled from average projections of 2–4 images or best focus images (each exposure 400 msec) acquired in stacks. Photobleaching of Alexa-488 Dam1 complexes was accomplished with the 488 nm line from an Argon ion laser (Melles Griot, series 532, model 35 LAS 450), optically connected with the microscope's epi-illumination path. To bleach static complexes on the MT walls (Fig. 2), the laser beam was focused into the 3–4 μm spot. To quantify the brightness, and therefore the size, of the tracking Alexa488-Dam1 complexes, we incubated our segmented MT with this protein to form stable fluorescent dots, induced MT depolymerization and confirmed Dam1 tracking with attenuated light from an HBO100 arc lamp, then turned on the Argon laser with defocused beam, as described in Supplement Part 2, and recorded the initial intensity of the tracking complex before it bleached.

Electron Microscopy. MTs were grown from unlabeled tubulin or its mixture with biotinylated tubulin (2.5:1) and stabilized with taxol. Formvar-coated, glow-discharged EM grids were additionally coated with the streptavidin layer, then allowed to bind biotinylated MTs for 5 min. This method should attach MTs uniformly to their substratum, inhibiting the subsequent formation of MT-surrounding rings. Dam1 (10–70 nM) in motility buffer was then added for 2 min, after which the grids were washed once with a protein-free buffer and lightly fixed by the addition of formaldehyde and gluteraldehyde (final concentrations 1% and 0.05%, respectively) for 2 min. These grids were washed with BRB80 and negatively stained with 2% Uranyl Acetate. To examine complexes formed on MTs suspended in the solution (Fig. 1B and 4D, panel iv), unlabeled MTs were incubated for 2 min in a solution of Dam1 (200–350 nM) in BRB80 with 1% βME, then applied to a Formvar-coated grid and stained with Uranyl Acetate. Specimens were imaged with an F20 electron microscope from FEI Inc (Eindhoven, NL).

Data Analysis. All numbers in figures are mean ± SEM, unless stated otherwise. Since most of the rate distributions are asymmetric and non-Gaussian ($P \geq 0.98$) (e.g., Fig. 3A), they were fitted with MatLab6.5 using the Rayleigh approximation

$$y = \frac{x}{a^2} e^{-\frac{x^2}{2a^2}}$$

or the sum of two such approximations to produce a fit with $P \geq 0.95$. Rates quoted in text are the positions of maximum peaks of these fits (parameter a) and their standard errors.

Part 2: Mathematical Analysis of the Kinetics of Photobleaching

To quantify the fluorescent intensity of Alexa488-Dam1 complexes, we flowed the protein in "motility" buffer into a microchamber topped with the acid-washed glass coverslip. The coverslip-attached dots were photobleached with Argon laser beam, which was defocused to illuminate ~ 30 μm circular area, and the intensities were recorded every 300 msec. To minimize the unevenness of illumination of the field of view we analyzed dots located close together in the central part of the field. The analysis was carried out on the dimmest dots, in which single steps could be detected more easily. Using similar approach we quantified bleaching of the coverslip-associated dots in experimental chambers, in which Dam1 end-tracking was also recorded.

Mathematical Analysis of the Photobleaching Curves. The recordings from each dot were first smoothed (average with the sliding window of 3 points). Then we subtracted the intensity of the background, acquired from a nearby area that was free of fluorescent dots. The resulting data were analyzed with two algorithms: Gaussian fitting (2) and the PDF-based algorithm (3). First, we tested the "null" hypothesis that our data represented gradual exponential photobleaching that was free of steps. Then, each of the algorithms was used to calculate the magnitude of the single bleaching step that would provide the best fit to the photobleaching curves.

Gaussian Fitting Algorithm. To test the null hypothesis we first averaged the curves from all experiments and fitted the resulting curve with an exponent (Fig. S4A). This curve was then modified with a theoretical noise function that fit a normal distribution and had a mean amplitude equal to that of the experimental noise. We generated 1000 of such randomly modified curves, plotted their intensity histograms and averaged them. The resulting histogram (Fig. S4B, blue) shows the distribution of intensities expected within the framework of the null hypothesis with the characteristics corresponding to our experimental conditions.

To generate the histogram for the experimental data, we built intensity histograms for each of the experimental curves, and then pooled them together (Fig. S4B, red). This histogram differed significantly from the theoretical histogram generated as above (χ^2 test, $P < 10^{-5}$), which implies that the experimental curves contain discrete steps. To identify the most likely size for this step we fitted the average experimental histogram with equidistant Gaussian functions, similar to described in (2) (Fig. 1G). The step size, which is equal to the distance between the peaks of two adjacent Gaussian curves of 15,800 ± 1,200 a.u. provided the best fitting of the experimental histogram, as determined by the method of least squares.

PDF-Based Algorithm. To confirm that our experimental curves contained discrete steps, we analyzed our data with an alternative method. First, we averaged 17 individual bleaching curves and fitted the resulting curve with a descending exponent, as above (Fig. S4A). Then we generated 17 theoretical curves by modifying the exponential curve with normal noise that had the same mean amplitude as our experimental curves. All resulting points were then pooled and used to calculate the pairwise differences of the intensities, as in (3). Such a procedure was repeated 100 times, and the resulting PDF histograms were averaged. The average histogram (Fig. 4SC, blue) describes the theoretical pairwise difference distribution for the null hypothesis.

The data points from 17 experimental curves ($n = 486$) were then pooled and used to generate the experimental PDF histogram (Fig. 4SC, red). According to the χ^2 test this histogram differed significantly from the theoretically determined distribution of the null hypothesis ($P < 10^{-5}$), so this method too reveals the presence of steps in the experimental data. The experimental PDF histogram was then fit with equidistant Gaussian curves (Fig. 4SD). The step size calculated with this algorithm was 16,362 ± 1,990 a.u., which is highly similar to the size obtained with the first method.

Part 3: Behavior of DAM1-Coated Bead in the Absence of Soluble DAM1: A Comparison of Our Results with Published Data

The experiments with Dam1-coated beads carried out in the absence of soluble Dam1 reported in refs. 4 and 5 have been thought to indicate weak Dam1-MT binding under the assumption that the beads were attached to MTs via rings (6). Several arguments were proposed to support this assumption; the most persuasive was the finding that the beads could not move over a segment of the MT that was attached to the coverslip (4). However, this argument is quite indirect, while other observations reported in this work suggest that the data in (4, 5) were obtained in the absence of ring formation.

(*i*) The interactions used to immobilize Dam1 on the surfaces of beads in both the cited papers and our own experiments are strong, noncovalent chemical bonds; it seems improbable that some Dam1 protein could then detach from these beads and form rings around the MTs. Indeed, we could not detect any green staining on MTs in the presence of these beads for 2 h at 32°C (our routine experimental conditions). During all this time, the beads remained brightly fluorescent, supporting our view that Dam1 remained stably attached to the beads.

(*ii*) Our rates of movement for lightly and intermediately covered beads in the absence of soluble Dam1 were similar to that reported in (4) when adjusted for the difference in experimental temperatures (7), suggesting that a similar mechanism was involved.

(*iii*) In the cited work, the authors report that not washing the unbound Dam1 away from the beads did not change their behavior (note, however, that neither the resulting concentration of soluble Dam1 nor evidence for the formation of MT-associated Dam1 complexes were reported for these conditions) (4, 5). In our assays, visible fluorescent dots formed along the MTs when soluble Dam1 was present (e.g., Fig. S2*A*), and the beads moved significantly slower than in the absence of soluble Dam1 (Fig. 3*A*).

The difference between these studies with respect to the effect of adding back the soluble Dam1 may have resulted from the presence of soluble tubulin in the published studies (4, 5) but not in our assays. When we added Alexa488-Dam1 to MTs in the presence of 13 μM soluble tubulin, using the "motility buffer" of our experiments, we could not detect any green dots on the MTs at concentrations of Alexa488-Dam1 that would have been sufficient to decorate MTs in tubulin's absence. It appears that soluble tubulin, which in *in vitro* assays is commonly in excess to polymerized tubulin, inhibits the formation of Dam1-MT complexes. This may explain why the experiments in (4) with washed and unwashed Dam1-beads gave identical results: most likely rings failed to form under both conditions.

(*iv*) If bead-associated Dam1 could somehow form rings around MTs, one would expect that beads with more bound Dam1 would move more slowly than beads associated with fewer

Dam1 molecules, because beads move slower in the presence of soluble Dam1. Our results, however, show the opposite effect (Fig. 3*B*).

(*v*) The buffers used in refs. 4 and 5 lacked strong reducing agents, which in our experiments were required for Dam1 diffusion and tracking of shortening MT ends but not for the motions of beads in the absence of soluble Dam1. With no βME in our assay the beads tracked MT shortening ends less processively, which is similar to the frequent bead detachment described in (4).

1. Wang HW, *et al*. (2007) Architecture of the Dam1 kinetochore ring complex and implications for microtubule-driven assembly and force-coupling mechanisms. *Nat Struct Mol Biol* 14:721–726.
2. Park M, Kim H-H, Kim D, Song NW (2005) Counting the number of fluorophores labeled in biomolecules by observing the fluorescence-intensity transient of a single molecule. *Bull Chem Soc Jpn* 78:1612–1618.
3. Block SM, Svoboda K(1995) Analysis of high resolution recordings of motor movement. *Biophys J* 68:230S–239S.
4. Asbury CL, Gestaut DR, Powers AF, Franck AD, Davis TN (2006) The Dam1 kinetochore complex harnesses microtubule dynamics to produce force and movement. *Proc Natl Acad Sci USA* 103:9873–9878.
5. Franck AD, *et al*. (2007) Tension applied through the Dam1 complex promotes microtubule elongation providing a direct mechanism for length control in mitosis. *Nat Cell Biol* 9:832–837.
6. Efremov A, Grishchuk EL, McIntosh JR, Ataullakhanov FI (2007) In search of an optimal ring to couple microtubule depolymerization to processive chromosome motions. *Proc Natl Acad Sci USA* 104:19017–19022.
7. Fygenson DK, Braun E, Libchaber A (1994) Phase diagram of microtubules. *Phys Rev E* 50:1579–1588.

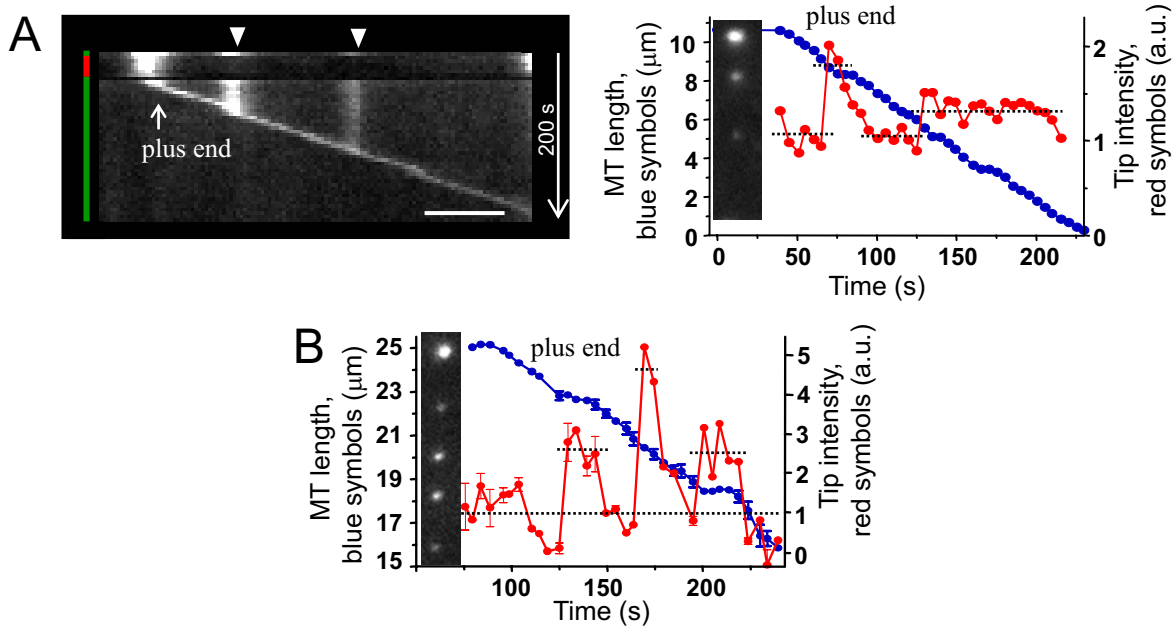

Fig. S1. When tubulin depolymerization reached an MT-associated, non-diffusing Dam1 complex, the steady movement of end-associated, or ''distal'' dot was usually interrupted by a short pause (e.g., at the brighter dot on the kymogram in *A*). The resumption of motion correlated with a decrease in brightness of the complex down to the level indicated with the lower dotted line on the graph, indicating depolymerization-induced loss of some Dam1. In other instances, brightness of the tip-associated Dam1 complex increased slightly when it approaches the dimmer Dam1 dots, while its movement continues uninterrupted (dimmer dot in *A*). (Scale bar, 2 μm.) *B* shows a MT with three static Dam1 dots. None was collected, and two caused noticeable pausing.

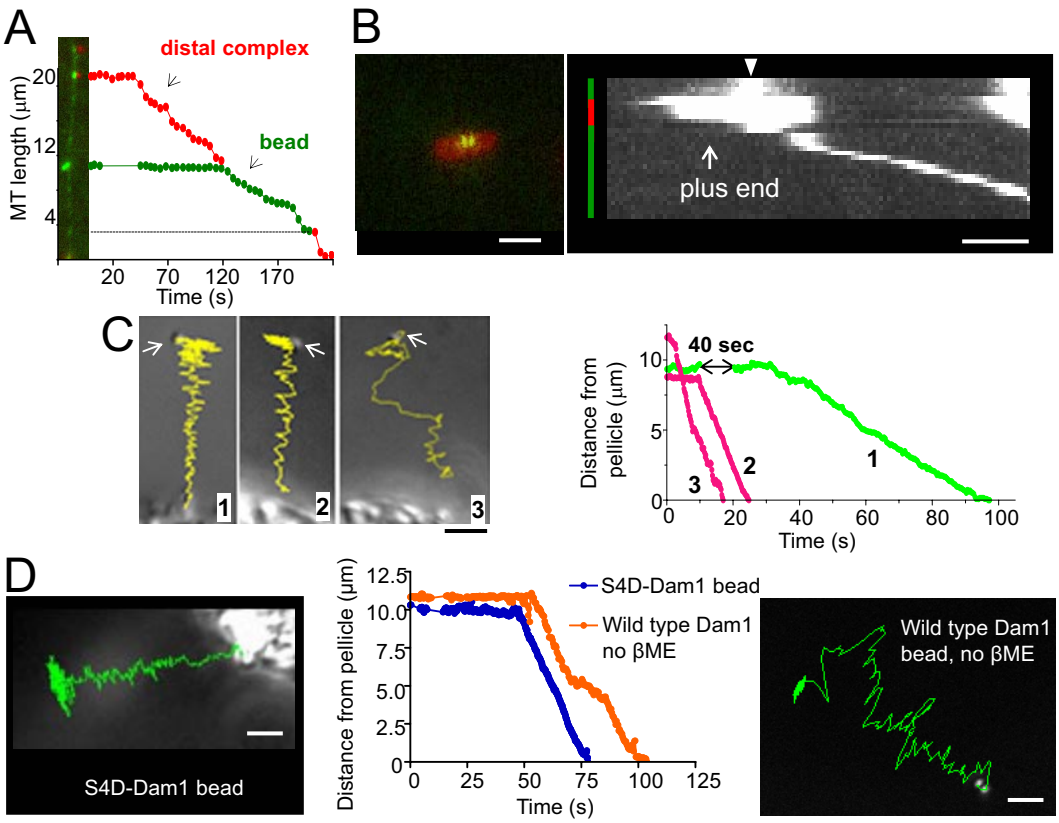

Fig. S2. (*A*) A Dam1-coated bead tracked a shortening MT end until it fell off at a spot of MT-associated Dam1 (black line). *Inset* shows the initial image with Dam1 decoration, attached bead (green), and MT cap (red). (*B*) Left image combines a DIC view of a Dam1-coated glass bead (green) and a red fluorescent image of the MT cap. As the MT cap disperses, this bead moves toward the MT's minus end at the axoneme in the absence of soluble Dam1, as shown on the kymograph (*Right*). About half of such cap-associated beads detached with photo-induced cap dissolution. Beads moved more frequently and more processively when we used *Tetrahymena* pellicles, probably because these nucleate denser arrays of MTs than axonemes, and bead attachment was stabilized by multiple MTs. Example trajectories (yellow) of Dam1-coated beads (*C Left*) and their graphs (*C Right*). Initial bead positions are indicated with white arrows; the pellicle is at the bottom of each DIC image. Bead #1 was observed in the presence of 16 nM Dam1, while beads #2 and 3 moved in the absence of soluble Dam1. In the presence of soluble Alexa488-Dam1, beads frequently attached to the GDP portion of the MTs, presumably through interaction between beads-associated Dam1 and Dam1 in the MT-associated dots. D. Beads coated with S4D-Dam1 complexes, which forms rings less efficiently than wild type Dam1 (1), also can track the end of depolymerizing MT in the absence of any soluble Dam1 (left). Beads coated with wild type Dam1 can follow the shortening MT end without soluble Dam1 even in the absence of βME (*Right*), consistent with the notion that these motions are ring independent. (Scale bars, 2 μm.)

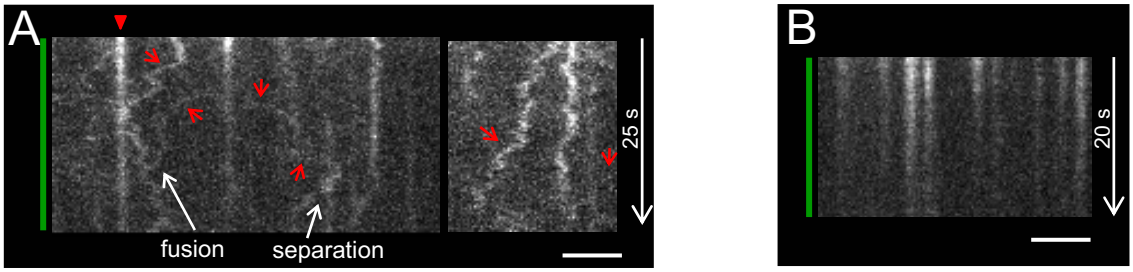

Fig. S3. (*A*) Thermal motions of Dam1 patches. On coverglass-attached, taxol-stabilized GDP MTs the weakly stained dots undergo fast random walks (red arrows; faster moving dots create lines closer to horizontal), while some, usually brighter, Dam1 complexes remain motionless (arrowhead). (*B*) Analogous experiment carried out without βME showed absence of detectable Dam1 diffusion. (Scale bars, 2 μm.)

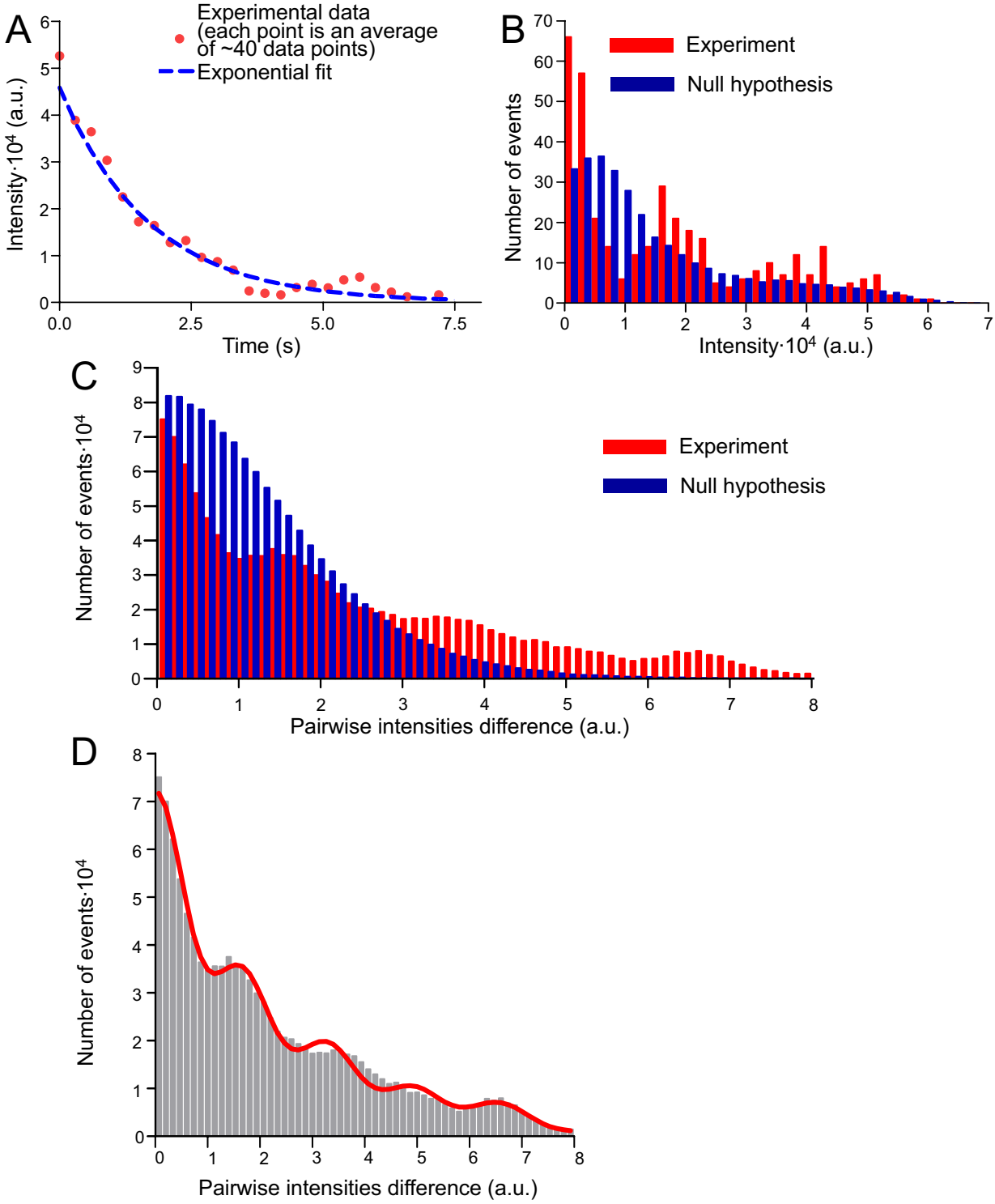

Fig. S4. (*A*) The kinetics of photobleaching (average of 44 experimental curves) and its exponential approximation. (*B*) Distributions of fluorescence intensities as seen in our experiments (red) and as expected from the null hypothesis of no steps in photobleaching (blue).(*C*) PDF histograms for experimental intensities (red) and theoretically generated on the basis of null hypothesis (blue). (*D*) Gaussian fitting (red line) of the experimental PDF histogram to identify the most probable size of a single step.

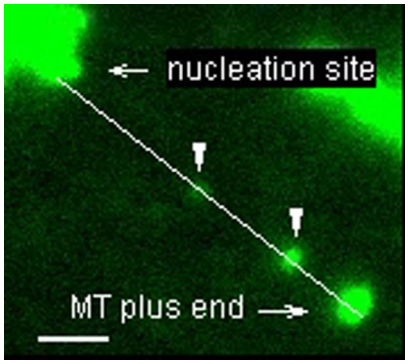

Movie S1. Movement of a Dam1 complex associated with the tip of a disassembling MT. MTs where grown from Chlamydomonas axonemes, capped, then washed and incubated with Alexa488-Dam1. Images in green were acquired with a GFP filter; red images show photo-induced depolymerization of the rhodaminated cap with light from a Texas red filter. Two Dam1 complexes on the GDP part of MT (arrowheads) show no motion until the arrival of the distal complex. (Scale bar, 2 μm.) This dot moves at 3 μm/min (Fig. S1*A*); the weaker dot on another MT in the upper part of the video moves at 6 μm/min (played 15$\times$ faster than recorded). The slow movement of the Dam1 dot and its relatively unchanged intensity appear to be features of Dam1 ring motility.

Movie S1.mov

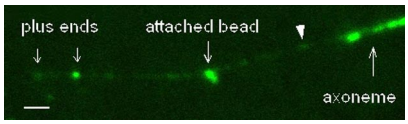

Movie S2. Bead movement under conditions permissive for ring assembly. MTs were grown as for Movie S1, then decorated with Alexa488-Dam1, and incubated with beads coated with Alexa488-Dam1. Arrowhead points to a Dam1 spot where the bead falls off. The quantified data are shown on Fig. S2*A*. Played 15× faster than recorded. (Scale bar, 2 μm.)

Movie S2.mov

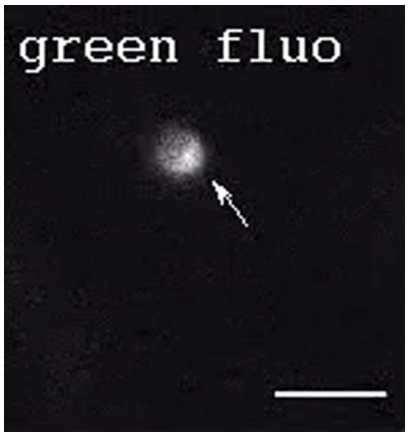

Movie S3. Sliding of the Dam1-coated bead in the presence of soluble Dam1. The experiment was carried out as in Movie S2. Images were acquired every 100 msec, using a GFP fluorescence filter to visualize the Alexa488-Dam1 spot on bead's surface. Played 1.5× faster than recorded. (Scale bar, 3 μm.)

Movie S3.mov

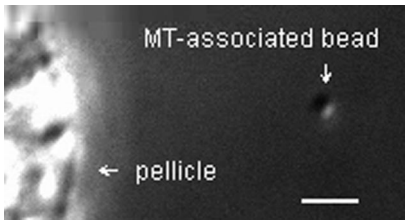

Movie S4. Transport of the Dam1-coated beads in the absence of ring-formation. MTs were grown from Tetrahymena pellicles and capped with rhodamine-labeled tubulin. The soluble tubulin was then washed away, and Alexa488 Dam1-coated beads were introduced into the chamber and allowed to bind the MTs. No green fluorescence could be detected on MTs anywhere in the chamber, so the labeled Dam 1 remained stably attached to the beads. After the GMPCPP MT caps were dispersed, bead movement was followed with DIC optics. A small particle is seen diffusing randomly in some of the video frames, but the attached bead's movements are not random. Its initial Brownian movements are almost parallel to the surface of the nearby pellicle, because they are restricted by the attached MT. Once MT depolymerization begins, the bead moves processively toward the pellicle at ~35 μm/min (played 2$\times$ faster than recorded). (Scale bar, 2 μm.)

Movie S4.mov

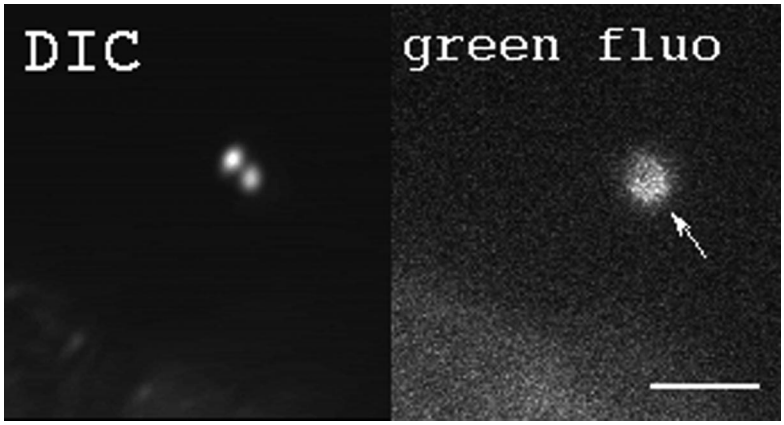

Movie S5. Rotational motions of a Dam1-coated bead in the absence of soluble Dam1. This experiment was carried out as in Movie S4 (in the absence of soluble Dam1), but the bead had a spot of brighter fluorescence on its surface. There is a short delay between visualizations in DIC (exposure 25 msec) and the fluorescent channel (exposure 50 msec), so bead positions in the corresponding frames are not identical. Images were acquired every 6 sec. (Scale bar, 3 μm.)

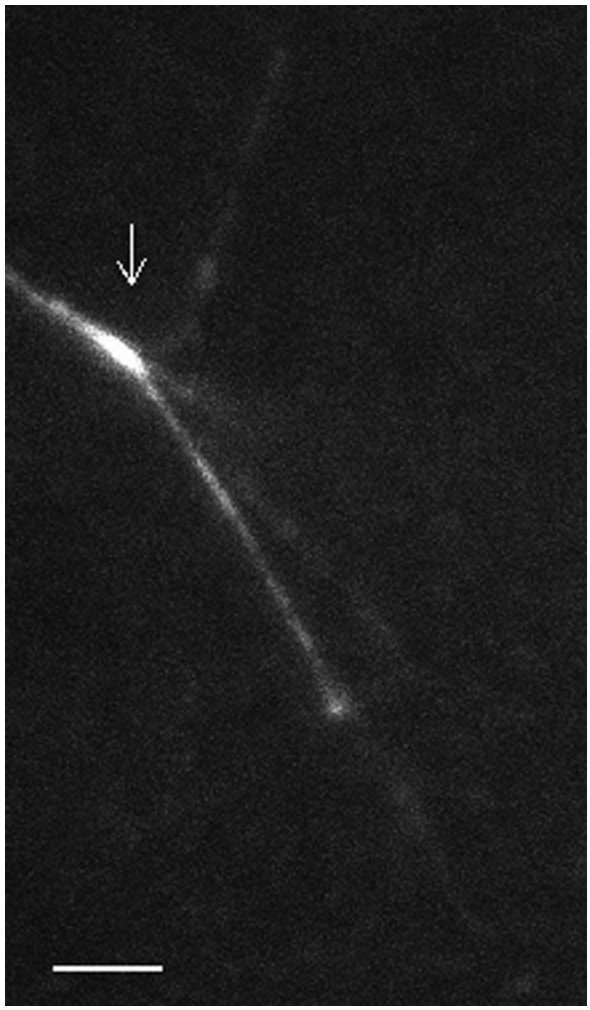

Movie S6. MT end-tracking and transduction of force by the S4D-Dam1 mutant complex. The experiment was carried out as in Movie S1 but using mutant S4D-Dam1, Alexa488-labeled protein. Brighter dots travel with the ends of several MTs that grew from one axoneme (arrow) and that depolymerize asynchronously. Images were acquired in stacks of 3 planes every 2 sec (150 msec exposure per plane). Video shows selected planes, so that focus is maintained on a bright junction between the shortening end of one MT and the wall of another, where a force-transducing attachment has formed. (Scale bar, 3 μm.)